Int. J. Adv. Appl. Math. and Mech. 2(3) (2015) 60 - 71 (ISSN: 2347-2529)
Journal homepage: www.ijaamm.com

IJAAMM

International Journal of Advances in Applied Mathematics and Mechanics

Modelling of shallow-water equations by using compact MacCormack-Type schemes with application to dam-break problem

Research Article

Samir K. Das[1, *], **Jafar Bagheri**[2]

[1]*Department of Applied Mathematics, Defence Institute of Advanced Technology,Deemed University, Girinagar, Pune, India*

[2]*Eslamabad-E-Gharab Branch, Islamic Azad University, Eslamabad-E-Gharab, Iran*

Received 14 January 2015; accepted (in revised version) 16 March 2015

Abstract: This paper investigates dam-break flow problem with the aim to capture fluid flow in transition to solve two-dimensional shallow-water equations (SWE). Applying compact MacCormack type schemes with high accuracy approach, governing equations are solved using one-sided implicit stencil with five-point explicit boundary stencil. Spatial derivatives are obtained numerically by solving a bi-diagonal matrix along the grid line instead three-diagonal matrix inversion. The model results are validated for dam-break flow problem and compared with the Stoker solution for one-dimensional case and experimental results of two-dimensional case. Considering various parameters for one-dimensional flow problem with respect to water depth and velocity, L_1 errors are computed for wet bed case using second order and fourth order MacCormack schemes. The comparison of L_1 errors with respect to the grid size and dissipative effect also analyzed for both the schemes. The model results are found be in good agreement with the analytical solution and experimental results for dry and wet bed conditions. The present model proved to more versatile even for the coarser grids and can provide a useful framework for spatial discretization.

MSC: 65M06 • 65M22 • 76B15 • 35L50

Keywords: SWE • HOC • MacCormack-type schemes • Dam-brak • Conservation-law • Explicit and Implicit schemes

1. Introduction

The dam-break is basically a catastrophic failure of dam, leading to uncontrolled release of water causing flood in the downstream region. The analysis of dam-break flow is important for dam design and safety. To model the dam break flow problems several researchers have investigated the flood wave caused due to dam-break either experimentally or numerically [1, 2]. Using the Eulerian frame of [2], numerically simulated two-dimensional flood wave propagation due to a dam failure where the velocity components, water depth and the position of water front for each time step are computed through an explicit finite difference scheme. Extending one- dimensional (1-D) approach based on characteristic equations, Katopodes [3] developed two-dimensional (2-D) numerical model for the dam-break flow problem. Fread and Lewis [4] developed a generalized flood routing model FLDWAV based on Preissman implicit scheme which can be used for a wide range of unsteady flow applications that includes flood forecasting in a dendritic river system and dam-breach analysis. Using the two step MacCormack predictor-corrector schemes, Bellos [5] examined 2-D dam-break flow problem numerically for transformed system of equations and the results are compared with the experimental data. Using a simple algebraic coordinate transformation technique, Mohapatra and Bhallamundi [6] simulated dam-break flow in channel transitions by

* Corresponding author.
E-mail address: samirkdas@diat.ac.in

applying the MacCormack finite difference scheme. For the better resolution of the flow properties, Rahman and Chaudhry [7] simulated dam-break flow with local grid adaptation technique for subcritical and the supercritical flows under extreme boundary conditions. Zoppou and Roberts [8] obtained numerical solution for unsteady dam-break flow problem using second-order approximate Riemann solver with a van-Leer type limiter on a Cartesian grid. This model is stable, robust and capable of resolving shocks, steep bed slopes and to handle complex geometry. Using the OpenFOAM and Reynolds-Averaged Navier-Stokes (RANS) equations coupled with Volume of Fluid (VOF) method, Biscarini et al. [9] numerically simulated three-dimensional free surface flow induced by dam-break. Using the method of characteristics, Bellos and Hrissanthou [5] developed two numerical models for 1-D SWE by using Lax-Wendroff and MacCormack schemes. Bagheri and Das [10] modeled 2-D unsteady SWE by using implicit higher order compact scheme (HOC) for dam-break flow problem and validated the result with the experimental results. Tandel and Bhathawala [11] derived a mathematical model for one-dimensional ground water recharge through porous media. Kumar and Arora [12] used the Reduced Differential Transform Method (RDTM) for solving the coupled system of Burgers' equations and coupled Klein Gordon Equation. Aslefallah and Rostamy [13] examined finite difference theta-method to solve Fractional Diffusion Differential Equations by using spatial extrapolation.

In recent years, higher-order compact (HOC) scheme has gained lot of importance as it uses smaller stencils and predicts more accurate results. The compact scheme is a class of higher order finite difference methods, which provides an effective way of joining spectral method for accuracy and robust characteristics of finite difference schemes. The compact scheme uses smaller stencil to approximate leading truncation error terms of the governing equation and to provide better resolution. The applications of compact scheme for various fluid flow problems can be obtained from the investigations [1, 14] Using the conservation-law form, Navon and Riphagen [1] developed fourth order compact algorithm by using alternating direction implicit finite-difference scheme to solve non-linear SWE. To solve the Euler equations, Abarbanel and Kumar [15] developed an unconditionally stable HOC scheme. By extending the high accuracy approximation method, Gupta [16] solved incompressible Navier-Stokes equation for lead driven cavity problem. Lele [17] has investigated higher order compact scheme for spectral-like resolution with the approximation of the first and second derivative and extending up to tenth order on a uniform grid. After extending the previous work of Li et al. [18] for steady Navier-Stokes equation, Li and Tang [19] developed fourth order accurate compact scheme for unsteady viscous flow problem. Pandit et al. [20] proposed an implicit HOC finite- difference scheme for 2-D unsteady Navier-Stokes equations in irregular geometries by using orthogonal grids. Using the artificial viscosity approach, Shah et al. [14] developed a time accurate upwind higher order accurate compact finite difference scheme to solve Navier-Stokes equations.

To compute unsteady flow specifically in the presence of discontinuity, inherent dissipation and stability, one such widely used method is MacCormack method [21], This technique has been used successfully to provide time-accurate solution for fluid flow and aeroacoustics problems. The applications of this technique to 1- D shock tube and 2-D acoustic scattering problems provide good result while comparing with the exact solution. MacCormack [21] introduced a simpler variation of Lax-Wendroff scheme [22] which is basically a two-step scheme with second order Taylor series expansion in time and fourth order in spatial accuracy. This scheme is computationally efficient and easy to implement which can be appropriate to obtain reliable results. By using this scheme with two nodes, the flow field can be simulated for unsteady open channel flow especially for dam break problem in the presence of discontinuity and strict gradient conditions. Further, to capture fluid flow in transition over long periods of time and distance, numerical spatial derivative are required to be determined in few grid points while error controlled can be accurately computed. Hixon and Turkel [23] extended MacCormack scheme [21] to implicit compact differencing scheme by splitting the derivative operator of a central compact scheme into one-sided forward and backward operators by developing a prefactrorization method. Using this prefactrorization method, implicit matrix is splitted into two independent upper and lower triangular matrices that are easier to invert. The bi-diagonal matrices are used to calculate spatial derivatives along a grid line which depends on the numerical derivatives of the neighboring points. The one-sided nature of this method is an essential advantage especially when severe gradients are present.

In the present study, we adopt the fourth order compact MacCormack-type scheme extended by Hixon and Turkel [23] to solve transient one and two -dimensional SWE. The distinct advantages of this scheme are high order accuracy associated with compact stencils which provides accurate numerical solution even for relatively coarser grids with good approximation of wave front and does not show noticeable oscillations. To demonstrate the application of higher order compact scheme for 2-D case, classical dam-break problem is considered to simulate the flood wave in channel transition. The results are validated with the Stoker [24] solution for 1-D case and experimental results of Townson and Al-Salihi [25] and numerical results of Bagheri and Das [10] for 2-D case. The paper is organized as follows: Section-2 provides the mathematical formulation. Section-3 discusses computation procedure and algorithm. Section-4 deals with the numerical results of various test cases for wet bed and dry bed conditions.

Fig. 1. 1(a): Definition sketch prior to dam-break 1(b): Definition sketch after dam-break

2. Mathematical modelling

A parallel-parallel channel with complete breach is considered by assuming the flow to be inviscid and incompressible and accordingly non-linear SWE are expressed as Fig. 1

$$\frac{\partial h}{\partial t}+\frac{\partial}{\partial x}(uh)+\frac{\partial}{\partial y}(vh)=0 \tag{1}$$

$$\frac{\partial}{\partial t}(uh)+\frac{\partial}{\partial x}(u^2h)+\frac{\partial}{\partial y}(uvh)=gh[S_{0_x}-\frac{\partial h}{\partial x}-S_{f_x}] \tag{2}$$

$$\frac{\partial}{\partial t}(vh)+\frac{\partial}{\partial x}(uvh)+\frac{\partial}{\partial y}(v^2h)=gh[S_{0_y}-\frac{\partial h}{\partial y}-S_{f_y}] \tag{3}$$

These above equations are described in primitive variable form which is obtained from NavierStokes (NS) equations by integrating over the depth and assuming hydrostatic pressure distribution. Further, vertical velocity component and corresponding shear stress is also considered insignificant.

The set of partial differential equations (PDEs) are nonlinear first-order and hyperbolic in nature. Here, h is water depth; u is depth averaged velocity in the x-direction; v is depth averaged velocity in the y- direction; g is acceleration due to gravity; S_{0_x} is bed slope in the x-direction; S_{0_y} is bed slope in the y-direction; S_{f_x} is bottom friction in the x-direction; S_{f_y} is bottom friction in the y- direction. The bottom friction can be estimated by using the Manning's formula:

$$S_{f_x}=\frac{n^2u\sqrt{u^2+v^2}}{c_0^2h^{1.3\bar{3}}} \quad and \quad S_{f_y}=\frac{n^2v\sqrt{u^2+v^2}}{c_0^2h^{1.3\bar{3}}} \tag{4}$$

where n is Manning's roughness coefficient; and c_0 is a dimensional constant. The governing equation (1-3) can be written in conservative law form or divergence form as

$$\frac{\partial \varphi}{\partial t}+\frac{\partial \mathbf{F}(\varphi)}{\partial x}+\frac{\partial \mathbf{G}(\varphi)}{\partial y}=\mathbf{S}(\varphi) \tag{5}$$

where $\varphi, \mathbf{F}(\varphi), \mathbf{G}(\varphi), \mathbf{S}(\varphi)$ are the column matrices

$$\varphi=\begin{pmatrix} h \\ hu \\ hv \end{pmatrix}, \mathbf{F}(\varphi)=\begin{pmatrix} uh \\ u^2h+\frac{gh^2}{2} \\ uvh \end{pmatrix}, \mathbf{G}(\varphi)=\begin{pmatrix} vh \\ uvh \\ v^2h+\frac{gh^2}{2} \end{pmatrix}, \mathbf{S}(\varphi)=\begin{pmatrix} 0 \\ gh(s_{0_x}-s_{f_x}) \\ gh(s_{0_y}-s_{f_x}) \end{pmatrix} \tag{6}$$

Here φ denotes a vector containing the primitive variables h, u, v; $\mathbf{F}(\varphi)$ and $\mathbf{G}(\varphi)$ are vectors written in flux form and are functions of φ; $\mathbf{S}(\varphi)$ is the source Term. The scheme developed here is in rectangular Cartesian coordinate system for the grid point (i, j) with two -time levels at n and $n+1$. We discretize equation (5) by adopting second order explicit MacCormack [21] and fourth order compact Implicit MacCormack schemes developed by Hixon [23].

3. Computational procedures and algorithm

Adopting MacCormack explicit finite difference time marching scheme which consists of two-step predictor-corrector sequence where the flow variables are known at n time level and their values are to be determined at $n+1$ time level. The combinations of backward and forward spatial finite difference correspond to four equivalent alternatives of the numerical scheme and their cyclic change which is correct with respect to inherent unevenness.
Predictor step :

$$\varphi^*_{i,j}=\varphi^n_{i,j}-\Delta t\frac{\partial \mathbf{F}^n(\varphi)}{\partial x}|^F_{i,j}-\Delta t\frac{\partial \mathbf{G}^n(\varphi)}{\partial y}|^B_{i,j}+\Delta t S^n_{i,j} \tag{7}$$

Corrector step :

$$\varphi_{i,j}^{n+1}=\frac{1}{2}[\varphi_{i,j}^{n}+\varphi_{i,j}^{*}-\Delta t\frac{\partial \mathbf{F}^{*}(\varphi)}{\partial x}|_{i,j}^{B}-\Delta t\frac{\partial \mathbf{G}^{*}(\varphi)}{\partial y}|_{i,j}^{F}+\Delta t S_{i,j}^{*}] \tag{8}$$

Here, the indexes F and B are indicated forward and backward difference of the spatial derivative respectively. In the predictor step, scheme uses forward and backwards operators to estimate $\frac{\partial \mathbf{F}^{n}(\varphi)}{\partial x}$ and $\frac{\partial \mathbf{G}^{n}(\varphi)}{\partial y}$ from known information at the time-level n and in the corrector step backward and forward operators are used to estimate $\frac{\partial \mathbf{F}^{*}(\varphi)}{\partial x}$ and $\frac{\partial \mathbf{G}^{*}(\varphi)}{\partial y}$ from known information at time-level* (one -sided operators opposite to the predictor step). In order to eliminate the bias difference operators are repeated in every fourth time step as shown in Table 1.

Table 1. Difference operator sequence

Time step	Predictor		corrector	
	x	y	x	y
1	F	B	B	F
2	B	F	F	B
3	F	F	B	B
4	B	B	F	F

According to equation (7), the predictor values for the h, u and v are computed. The spatial derivatives $\frac{\partial \mathbf{F}^{n}(\varphi)}{\partial x}$ and $\frac{\partial \mathbf{G}^{n}(\varphi)}{\partial y}$, can be determined by second and forth order scheme as follows.

3.1. Explicit second order MacCormack scheme

The spatial derivatives for forward and backward difference operators can be expressed as

$$\begin{aligned}\frac{\partial \mathbf{F}^{n}(\varphi)}{\partial x}|_{i+1,j}^{F}&=(\frac{1}{\Delta x})(\mathbf{F}_{i+1,j}^{n}(\varphi)-\mathbf{F}_{i,j}^{n}(\varphi))\\ \frac{\partial \mathbf{F}^{n}(\varphi)}{\partial x}|_{i-1,j}^{B}&=(\frac{1}{\Delta x})(\mathbf{F}_{i,j}^{n}(\varphi)-\mathbf{F}_{i-1,j}^{n}(\varphi))\end{aligned} \tag{9}$$

$$\begin{aligned}\frac{\partial \mathbf{G}^{n}(\varphi)}{\partial y}|_{i,j+1}^{F}&=(\frac{1}{\Delta y})(\mathbf{G}_{i,j+1}^{n}(\varphi)-\mathbf{G}_{i,j}^{n}(\varphi))\\ \frac{\partial \mathbf{G}^{n}(\varphi)}{\partial y}|_{i,j-1}^{F}&=(\frac{1}{\Delta y})(\mathbf{G}_{i,j}^{n}(\varphi)-\mathbf{G}_{i,j-1}^{n}(\varphi))\end{aligned} \tag{10}$$

To adopt second order scheme we first obtain intermediate value $\varphi_{i,j}^{*}$ from known values at the nth time-level by using equation (7) and before that spatial derivative are computed by using equation (9) and (10) . Subsequently, values of $\varphi_{i,j}^{n+1}$ at $n+1$ time level are obtained by using equation (8). The stability criterion is defined by the Courant-Friedrichs-Lewy (CFL) condition [26].

$$\Delta t \leqslant min[\frac{\Delta x}{(u+\sqrt{gh})_{max}},\frac{\Delta y}{(v+\sqrt{gh})_{max}}) \tag{11}$$

To reduce the higher order dissipation due to aliasing error, dissipative term is added as Helfrich et al. [27].

$$D=\nu(0,\nabla.h\nabla u,\nabla.h\nabla v)^{T} \tag{12}$$

where the dissipative parameter ν is determined by using numerical experiments. To calculate the operations $\nabla.$ and ∇ can be used by the forward and backward operators. The spatial derivative at the boundary is computed by using two point one - sided explicit methods as follow:

$$\begin{aligned}\frac{\partial \varphi}{\partial x}|_{imax}&=\frac{1}{\Delta x}(\varphi_{i,j}-\varphi_{i-1,j})=0\\ \frac{\partial \varphi}{\partial x}|_{imin}&=\frac{1}{\Delta x}(\varphi_{i+1,j}-\varphi_{i,j})=0\end{aligned} \tag{13}$$

3.1.1. Solution algorithm

- Step 1: Initialize the height and velocity fields
- Step 2: Evaluate the values $\frac{\partial \mathbf{F}^n}{\partial x}$ and $\frac{\partial \mathbf{G}^n}{\partial y}$ by using equations (9) and (10)
- Step 3: Evaluate intermediate value $\varphi^*_{i,j}$ by using (7)
- Step 4: Evaluate the values $\frac{\partial \mathbf{F}^*}{\partial x}$ and $\frac{\partial \mathbf{G}^*}{\partial y}$ by using equations (9) and (10)
- Step 5: Evaluate the new value for the vector $\varphi^{n+1}_{i,j}$ at time level $n+1$ by using (8).
- Step 6: Evaluate the new value for boundary by using (13)
- Step 7: Calculate dissipative term by using (12), and then add to $\varphi^{n+1}_{i,j}$
- Step 8: Increase time step by Δt , if $t \le t_{max}$ go to Step 2.
- Step 9: End

3.2. Implicit fourth order compact MacCormack scheme

A general compact spatial derivative of a function f can be expressed as Hixon and Turkel [23].

$$[B]\{D\} = \frac{1}{\Delta x}[C]\{f\} \tag{14}$$

Here, D is the numerical approximation of the spatial derivative of the function f ,$[C]$ is the matrix of explicit coefficients and $[B]$ is the matrix of implicit coefficients which must be inverted to obtain D. As the values of D at a given point depends on the values of neighboring points of D, a tridiagonal matrix can be solved to obtain the special derivative

$$\{D\} = [B]^{-1}(\frac{1}{\Delta x}[C]\{f\}) \tag{15}$$

To achieve compact MaCcormack-type Scheme, the derivative operator is split into forward and backward operators such that

$$\{D\} = \frac{\{D^F\} + \{D^B\}}{2} \tag{16}$$

Here, D^F and D^B are one-sided forward and backward difference of the spatial derivative respectively. By using Taylor series expansion, fourth order compact operator along forward and backward direction for the spatial derivatives are defined as

$$\begin{aligned} aD^F_{i+1} + (1-a)D^F_i &= (\frac{1}{\Delta x})(f_{i+1} - f_i) \\ aD^B_{i-1} + (1-a)D^B_i &= (\frac{1}{\Delta x})(f_i - f_{i-1}) \end{aligned} \tag{17}$$

where $a = \frac{1}{2} \pm \frac{1}{2\sqrt{3}}$. The numerical spatial derivative determined by solving bi-diagonal matrix along the grid line [23] Using Taylor series expansion of the forward and backward operator gives

$$\begin{aligned} D^F &= \frac{\partial f}{\partial x} + \Delta x \frac{\sqrt{3}}{6}\frac{\partial^2 f}{\partial x^2} - (\Delta x)^3 \frac{\sqrt{3}}{72}\frac{\partial^4 f}{\partial x^4} + O(\Delta x)^4 \\ D^B &= \frac{\partial f}{\partial x} - \Delta x \frac{\sqrt{3}}{6}\frac{\partial^2 f}{\partial x^2} + (\Delta x)^3 \frac{\sqrt{3}}{72}\frac{\partial^4 f}{\partial x^4} + O(\Delta x)^4 \end{aligned} \tag{18}$$

The expressions for $\frac{\partial F^n(\varphi)}{\partial x}$ and $\frac{\partial G^n(\varphi)}{\partial y}$ are calculated by using equation (17)

$$\begin{aligned} a\frac{\partial \mathbf{F}^n(\varphi)}{\partial x}|^F_{i+1,j} + (1-a)\frac{\partial \mathbf{F}^n(\varphi)}{\partial x}|^F_{i,j} &= (\frac{1}{\Delta x})(\mathbf{F}^n_{i+1,j}(\varphi) - \mathbf{F}^n_{i,j}(\varphi)) \\ a\frac{\partial \mathbf{F}^n(\varphi)}{\partial x}|^B_{i-1,j} + (1-a)\frac{\partial \mathbf{F}^n(\varphi)}{\partial x}|^B_{i,j} &= (\frac{1}{\Delta x})(\mathbf{F}^n_{i,j}(\varphi) - \mathbf{F}^n_{i-1,j}(\varphi)) \end{aligned} \tag{19}$$

$$\begin{aligned} a\frac{\partial \mathbf{G}^n(\varphi)}{\partial y}|^F_{i,j+1} + (1-a)\frac{\partial \mathbf{G}^n(\varphi)}{\partial y}|^F_{i,j} &= (\frac{1}{\Delta y})(\mathbf{G}^n_{i,j+1}(\varphi) - \mathbf{G}^n_{i,j}(\varphi)) \\ a\frac{\partial \mathbf{G}^n(\varphi)}{\partial y}|^B_{i,j-1} + (1-a)\frac{\partial \mathbf{G}^n(\varphi)}{\partial y}|^B_{i,j} &= (\frac{1}{\Delta y})(\mathbf{G}^n_{i,j}(\varphi) - \mathbf{G}^n_{i,j-1}(\varphi)) \end{aligned} \tag{20}$$

For fourth order compact implicit scheme, the CFL condition is defined by multiplying 0.57 in equation (11).

$$\Delta t \leq min(\frac{\Delta x}{(u+\sqrt{gh})_{max}}, \frac{\Delta y}{(v+\sqrt{gh})_{max}}) * 0.57 \tag{21}$$

To reduce the higher order dissipation due to aliasing error introduced by the fourth-order compact scheme, dissipative term is added as mentioned in equation (12). To solve equation (5) following computational procedures are adopted. We first obtain intimidate value $\varphi^*_{i,j}$ from known values at the nth time-level by using equation (7) and before that spatial derivative are computed by using equation (19) and (20). Subsequently, values of $\varphi^{n+1}_{i,j}$at $n+1$ time level are obtained by using equation (8). The coefficient matrix in algebraic systems is obtained from equation (17) which is bi-diagonal for each grid line. The spatial derivative at the boundary is computed by using five point one-sided explicit methods with fourth order accuracy [23].

$$\begin{aligned}
\mathbf{D}^F_{imin} &= (-\frac{25}{12}+\frac{17}{12\sqrt{3}})f_i + (4-\frac{25}{6\sqrt{3}})f_{i+1} - (3-\frac{3\sqrt{3}}{2})f_{i+2} + (\frac{4}{3}-\frac{13}{6\sqrt{3}})f_{i+3} - (\frac{1}{4}-\frac{5}{12\sqrt{3}})f_{i+4} \\
\mathbf{D}^B_{imin} &= -(\frac{25}{12}+\frac{17}{12\sqrt{3}})f_i + (4+\frac{25}{6\sqrt{3}})f_{i+1} - (3+\frac{3\sqrt{3}}{2})f_{i+2} + (\frac{4}{3}+\frac{13}{6\sqrt{3}})f_{i+3} - (\frac{1}{4}+\frac{5}{12\sqrt{3}})f_{i+4}
\end{aligned} \tag{22}$$

$$\begin{aligned}
\mathbf{D}^F_{imax} &= (\frac{25}{12}+\frac{17}{12\sqrt{3}})f_i - (4+\frac{25}{6\sqrt{3}})f_{i-1} + (3+\frac{3\sqrt{3}}{2})f_{i-2} - (\frac{4}{3}+\frac{13}{6\sqrt{3}})f_{i-3} + (\frac{1}{4}+\frac{5}{12\sqrt{3}})f_{i-4} \\
\mathbf{D}^B_{imax} &= (\frac{25}{12}-\frac{17}{12\sqrt{3}})f_i - (4-\frac{25}{6\sqrt{3}})f_{i-1} + (3-\frac{3\sqrt{3}}{2})f_{i-2} - (\frac{4}{3}-\frac{13}{6\sqrt{3}})f_{i-3} + (\frac{1}{4}-\frac{5}{12\sqrt{3}})f_{i-4}
\end{aligned} \tag{23}$$

3.2.1. Solution algorithm

- Step 1: Initialize the height and velocity fields
- Step 2: Evaluate the values $\frac{\partial \mathbf{F}^n}{\partial x}$ and $\frac{\partial \mathbf{G}^n}{\partial y}$ by using equations (19) and (20) and before that boundary value are evaluated by using equation (22)
- Step 3: Evaluate intermediate value $\varphi^*_{i,j}$ by using (7)
- Step 4: Evaluate the values $\frac{\partial \mathbf{F}^*}{\partial x}$ and $\frac{\partial \mathbf{G}^*}{\partial y}$ by using equations (19) and (20) and before that boundary value are evaluated by using equation (22) and (23)
- Step 5: Evaluate the new value for the vector $\varphi^{n+1}_{i,j}$ at time level $n+1$ by using (8)
- Step 6: calculate dissipative term by using (12) and then add to $\varphi^{n+1}_{i,j}$
- Step 7: Increase time step by Δt , if $t \leq t_{max}$ go to Step 2
- Step 8: End

4. Results and discussions

In this problem, dam breach takes place instantaneously with full breach condition. Due to discontinuous initial conditions, it enforces several restrictions and most of the numerical schemes fail to capture this phenomenon. The algorithm developed here is second order accurate in time and fourth order accurate in space which the spatial derivative determined by a bidiagonal matrix along a grid line and using fourth order five-point non-centered difference at the wall boundaries. Interpolation has been performed along y direction while plotting. We present our results for wet bed and dry bed conditions for downstream of the dam. The actual water depth at $t = 0$ is specified as the initial condition in the downstream. The tail water / reservoir ratio for 1-D case with respect to wet bed and dry bed is considered as 0.5 and 0.0018 and for 2-D case 0.176 and 0.0014 respectively. In the case of dry bed, downstream water level below to this level would cause blow up due to not satisfying the continuity equation.

4.1. One dimensional (1-D) case

In this section, we consider 1-D dam break flow problem by considering that solid wall between upstream and downstream which collapse instantaneously Fig. 2.
In this problem, a horizontal channel (without slope and frictionless Bed) of length 1m with wall at either end is considered, dam wall is located at middle of channel which breaks instantaneously at time $t = 0$. The upstream water depth is $h_u = 1m$ and downstream water depths are $h_d = 0.5m$ and $0.018m$ for dry and wet bed respectively with zero initial velocity. Numerical simulations are carried out for wet bet and dry bed conditions and comparison

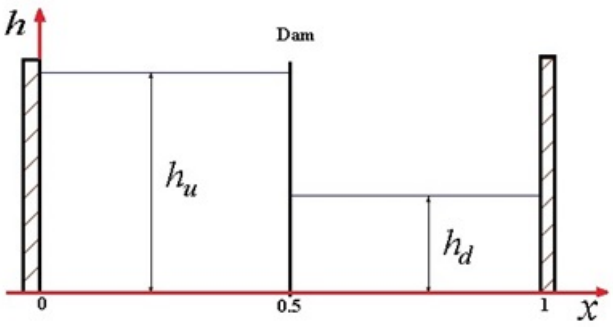

Fig. 2. Schematic diagram 1-D case prior to dam-break

are carried out with the analytical solution of Stoker [24]. However, comparisons are carried out only for wet bed condition with respect to velocity and water depth. Using open boundary condition, two solution methods are adopted: $(i)2^{\text{nd}}$ order explicit MacCormack scheme and $(ii)4^{\text{th}}$ order compact implicit MacCormack scheme. Numerical simulations are performed by considering $\Delta x = 0.01s$ with 100 grid points and the corresponding grid size is taken as $\Delta x = 0.01m$ along $x-$ direction. Fig. 3 (a-c). shows the water depth and velocity profiles at time $t = 0.1s$ after the dam-break for both the schemes. The comparison of numerical and analytical solution corresponding to water depth profile as well as velocity profile shows good agreement. It is observed that 4^{th} order compact implicit scheme provides better result than the 2^{nd} order explicit scheme as noticed in the depth profile Fig. 3 (a-c) as well as velocity profile Fig. 3 (d-f) . While comparing numerical and analytical result, minor oscillation is noticed in velocity profile while using 2^{nd} order explicit scheme which is primarily due to the lack of shock capturing ability. Fig. 4(a-e) shows comparison of depth profile for different depth ratio of the tail water to reservoir depth at $t = 0.1s$ after the dam-break. Five depth ratios were considered for simulation: $(a)\frac{h_u}{h_d} = 0.25, (b)\frac{h_u}{h_d} = 0.1, (c)\frac{h_u}{h_d} = 0.05, (d)\frac{h_u}{h_d} = 0.025, (e)\frac{h_u}{h_d} = 0.018$, and comparison was made with the analytical solution of Stoker [24]. Although, the depth profiles of 2^{nd} order and 4^{th} order scheme matches well with the analytical solution, 4^{th} order compact implicit scheme prove to be more efficient. With the decrease of depth ratio both the results improves significantly, except near the shock where 2^{nd} order scheme is found be less efficient Fig. 4 (a-e). As the depth ratio becomes minimum $\frac{h_u}{h_d} = 0.018$, 2^{nd} order scheme near the shock shows moderately high oscillation Fig. 4 (e).

Table 2. Difference operator sequence

Grid Number	Grid Spacing	Dissipative Parameter (ν)		L_1 Error (depth)		L_1 Error (velocity)	
N	Δx	$Mac4^{th}$	$Mac2^{th}$	$Mac4^{th}$	$Mac2^{th}$	$Mac4^{th}$	$Mac2^{th}$
50	0.02	9.00E-06	4.00E-05	0.0089	0.0199	0.0337	0.0723
100	0.01	5.00E-05	1.50E-05	0.0051	0.0104	0.0194	0.0374
200	0.005	1.00E-06	4.00E-06	0.0031	0.0043	0.0114	0.0152

Table 2 presents comparison of error for wet bed based on L_1 norm as an accuracy test for water depth and velocity at various grid sizes. With the increase of grid numbers, the difference of L_1 depth error and L_1 velocity error for 4^{th} order and 2^{nd} order schemes are almost marginal. The dissipative parameter ν depends on the grid size and determined by the numerical experiments. It is observed that the value of dissipative parameter is high up to N=100 girds for 4^{th} order scheme in comparison to 2^{nd} order scheme and subsequent increase of number of grids (N=200) dissipative parameter value decreases for 4^{th} order scheme in comparison to 2^{nd} order scheme. This indicates that dissipative effect is quite suitable for large grid spacing while applying 4^{th} order scheme. On the contrary, when the grid spacing is small 2^{nd} order scheme is well applicable. The L_1 norm can be defined as

$$error_N(L_1) = \sum_{i=1}^{N} \frac{|u_i - u_i^{ext}|}{N} \tag{24}$$

where u_i and u_i^{ext} are the computed and exact solution in i grid and N is the total number of grids. Also at the vicinity points of the shock are used to measure the errors which lead to relatively large errors.

4.2. Two dimensional (2-D) Case

To demonstrate the validity and effectiveness of the proposed scheme, unsteady 2-D dam-break flow problem in straight walled transition is considered. The schematic diagram of prior and after dam-break flow in straight walled

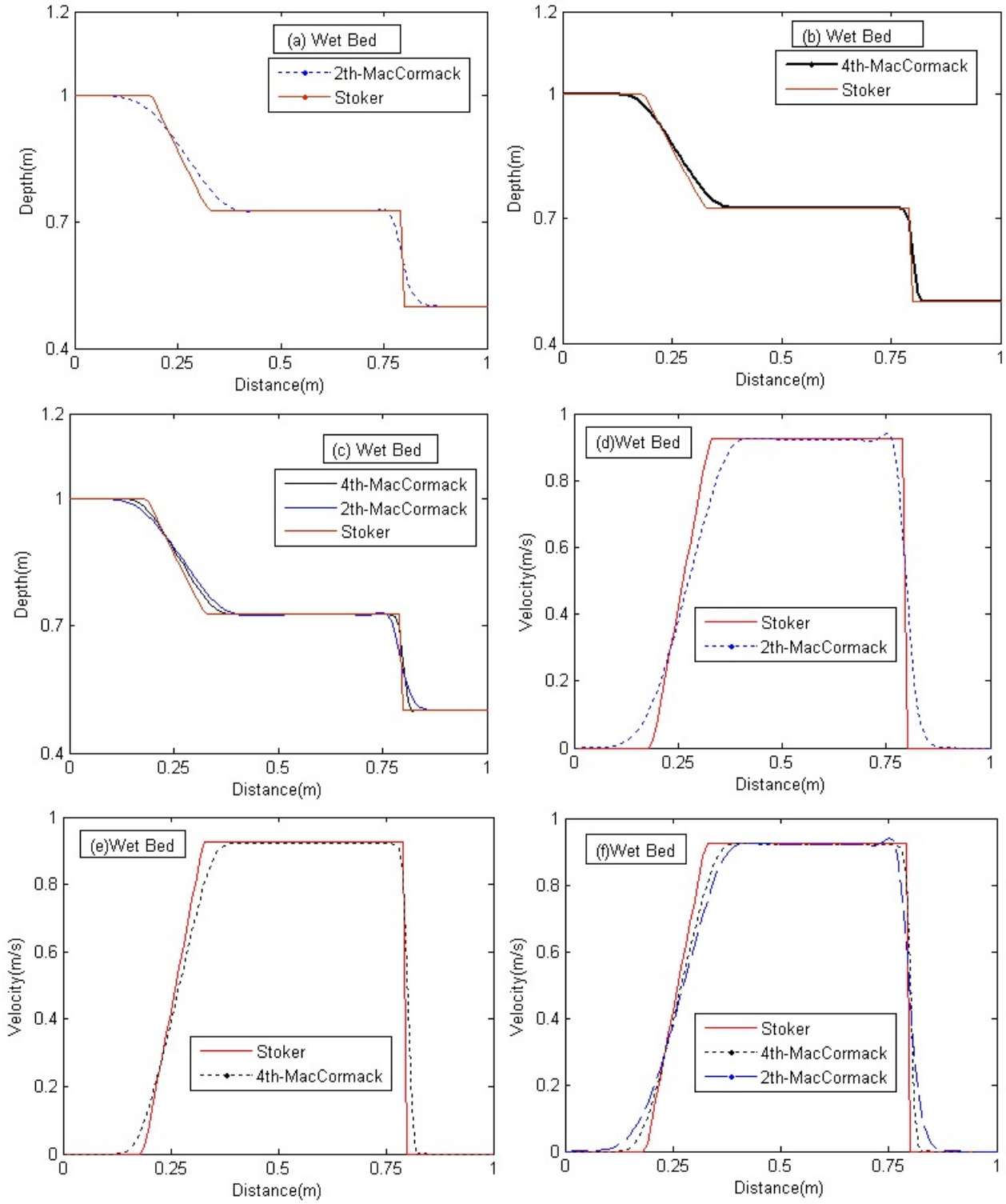

Fig. 3. Wet Bed: (a)-(c) Comparison of depth vs. distance, (d)-(f) Comparison of velocity vs. distance at $t = 0.1$

channel transition is shown in Fig. 1 (a, b). Townson and Al-Salihi [25] developed dam-break flow model for parallel, converging and diverging boundaries using the method of characteristics. Numerical computations are carried out based on the input values which correspond to the experiments conducted by Townson and Al-Salihi [25]. The computational domain comprises of $4m$ long and $0.1m$ wide channel and upstream length of the dam is $1.8m$ and downstream length is $2.2m$. The initial flow depth on the upstream side of the dam is $0.1m$ for both wet bed and dry bed whereas downstream water depth was assumed to be $0.0176m$ and $0.0014m$ respectively. The velocities u and v at the inflow boundary are specified as zero for all times and the flow depth at this boundary is computed by

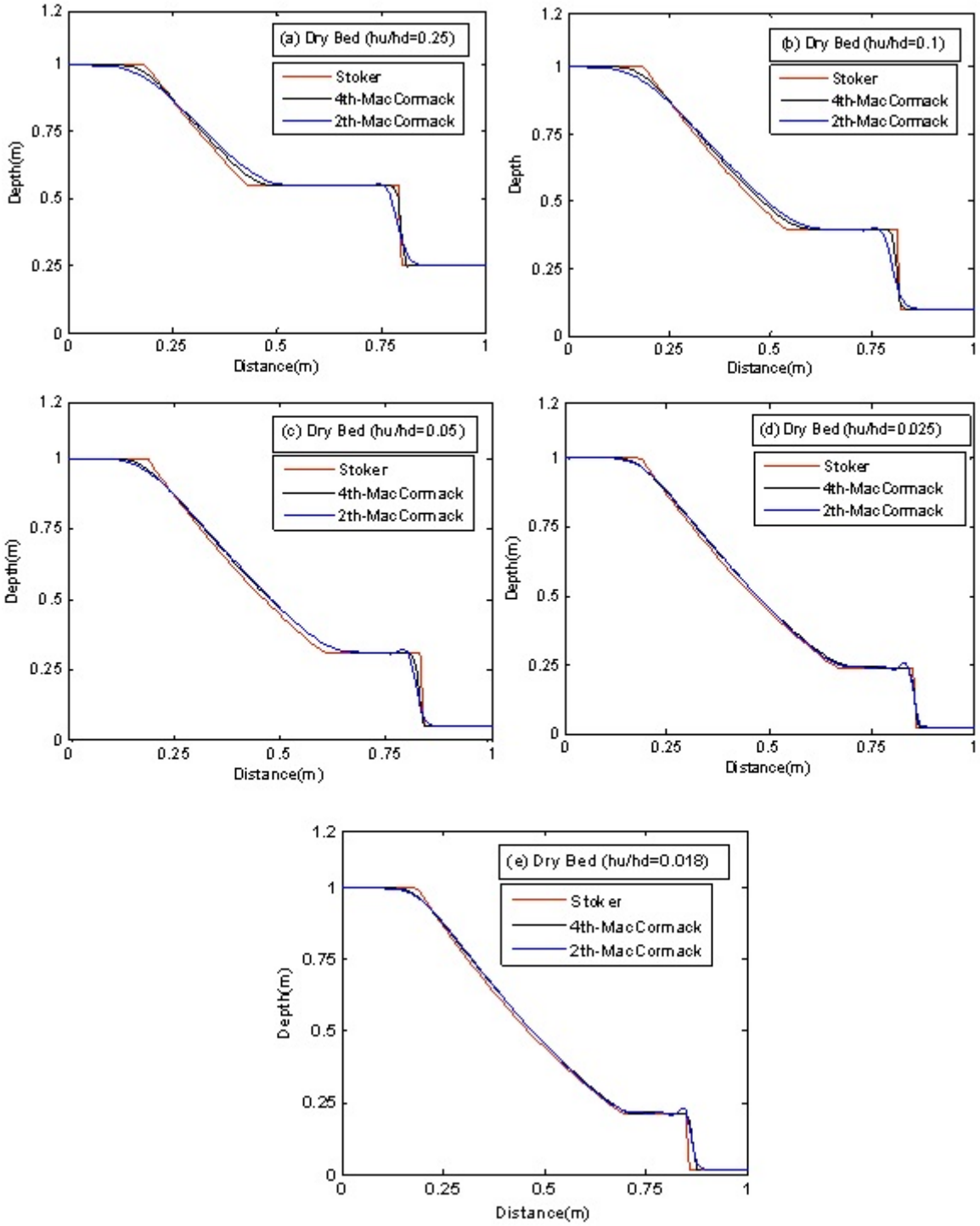

Fig. 4. Comparison of depth vs. distance for different ratios of the tail water to reservoir depths at $t = 0.1s$ for the dry bed conditions: (a) $\frac{h_u}{h_d} = 0.25$ (b) $\frac{h_u}{h_d} = 0.1$ (c) $\frac{h_u}{h_d} = 0.05$ (d) $\frac{h_u}{h_d} = 0.025$(e) $\frac{h_u}{h_d} = 0.018$

using the following linear extrapolation [6].

$$h_{1j}^{k+1} = 2h_{2j}^{k+1} - h_{3j}^{k+1} \tag{25}$$

The boundary conditions at the downstream end are same as initial condition in terms of depth and velocities. The symmetry boundaries are considered at the sidewalls. A higher order compact finite difference implicit scheme is used for numerical simulation for 81×81 grids with $\Delta t = 0.01$. The corresponding grid sizes become $\Delta x = 0.05m$ and $\Delta y = 0.0143m$ along x and y directions respectively. To reduce the higher order dissipation due to aliasing error introduced by the fourth-order compact scheme, we have added dissipative term Helfrich [27]. The numerical wave profiles are compared with the experimental results for $t = 2.5s$ after the instantaneous dam-break for the

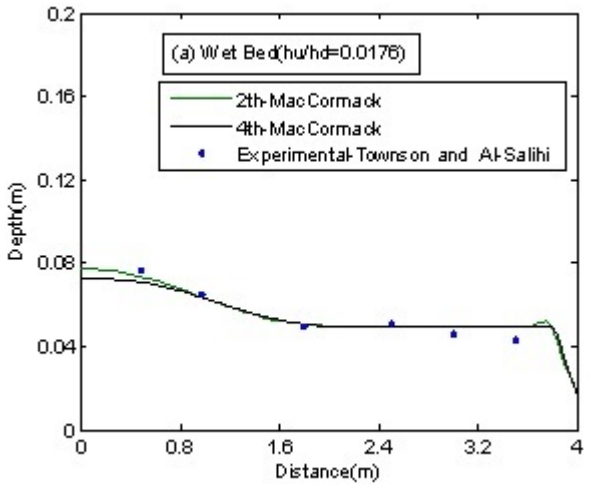

Fig. 5. Comparison of Depth vs. Distance: Wet-Bed at $t = 2.5$, $\frac{h_u}{h_d} = 0.0176$

wet bed conditions whereas for the dry bed condition $t = 1.5s$ is considered. Fig. 5 shows very good agreement of the water surface profiles between numerical and experimental results for wet bed condition in the vicinity of wave front. The upstream results are under measured due to dissipation. For dry bed condition various depth ratios are considered: $(a)\frac{h_u}{h_d} = 0.0014, (b)\frac{h_u}{h_d} = 0.002, (c)\frac{h_u}{h_d} = 0.0025$ and the result shows very good agreement for upstream section and also closer to the downstream boundary. The comparison of all three cases indicates that lowest depth ratio Fig. 6 (a) provides better results although noticeable oscillations are observed for all the cases near the shock Fig. 6 (a-c). However, in all the cases compact formulation provides much better results as compared to the results of second order case. With such coarser discretization, desired accuracy has been achieved in comparison to the traditional schemes. In the wet bed case for $t = 2.5s$, wave front height is higher than the measured one for both 2^{nd} and 4^{th} schemes, although higher order compact scheme adopted by Bagheri and Das [10] provides better result as observed from Fig. 7 (a) . Wave front for dry bed tracked closely by 4^{th} order 2^{nd} schemes for $t = 1.5s$ showing marginal difference in both the schemes. It is observed that both the schemes overestimate the result in comparison to experimental values whereas the results obtained by Bagheri and Das [10] provide accurate solution. The comparison of wet bed and dry bed indicates that both the scheme provides better results for wet bed case and difference is marginal. Fig. 7 (b) shows that near the dam wall, wave front for the dry bed condition some deviation is noticed for both the schemes in comparison to experimental results of Townson and Al-Salihi [25] and higher order compact numerical scheme [10].

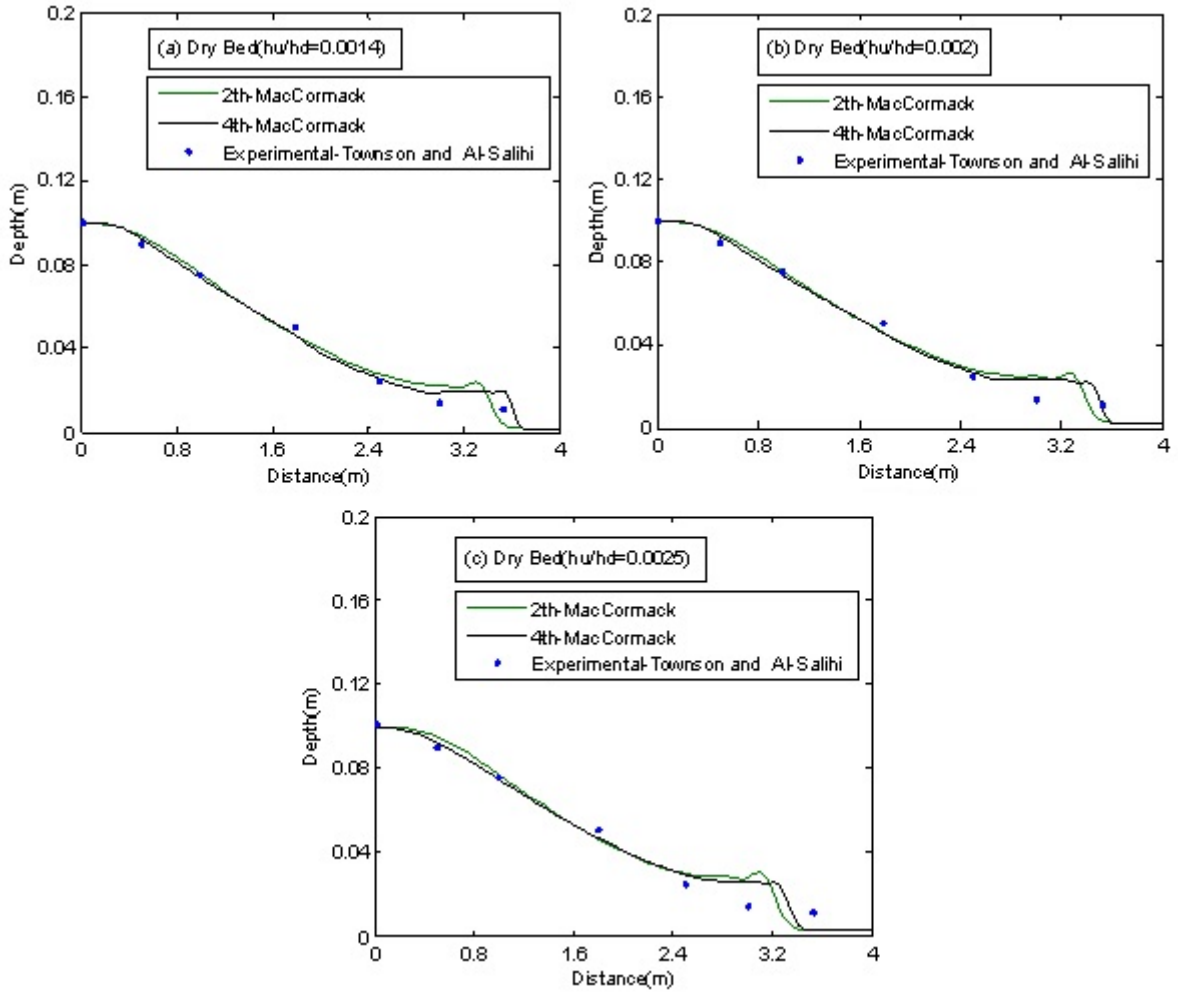

Fig. 6. (a): Dry-Bed at $t = 1.5, \frac{h_u}{h_d} = 0.0014$ (b-c): Comparison of Depth vs. Distance: (b) Dry-Bed at $t = 1.5, \frac{h_u}{h_d} = 0.002$(c) Dry-Bed at $t = 1.5$ and $\frac{h_u}{h_d} = 0.0025$

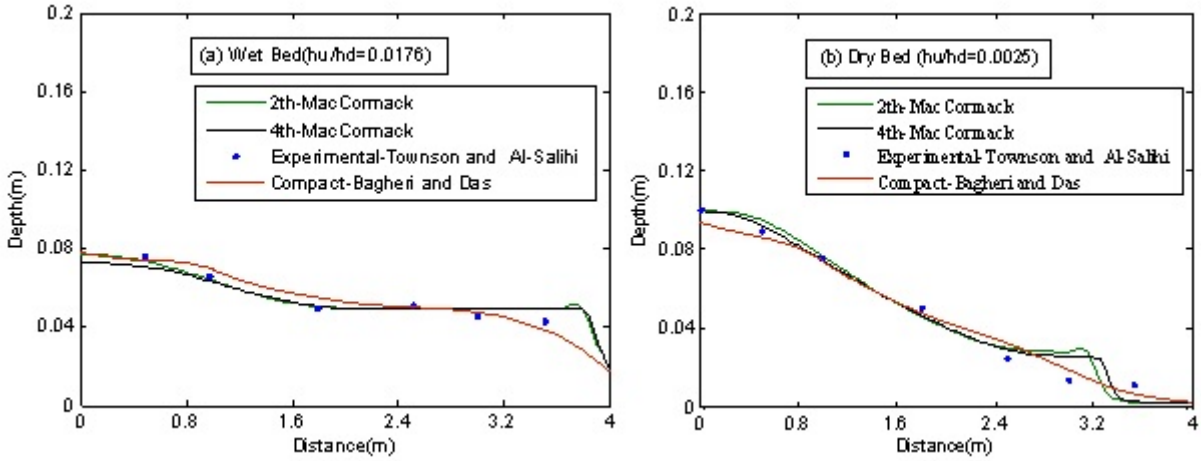

Fig. 7. Comparison of depth vs. distance: (a) Wet-Bed at $t = 2.5$ (b) Dry-Bed at $t = 1.5$

5. Conclusions

In this paper we have used two types of MacCormack schemes one is traditional second order and another one is compact fourth order schemes for unsteady case using conservative law form for $1-D$ and $2-D$ SWE. This fourth order compact scheme is applied for dam-break problem and the numerical results are compared with the

experimental result and exact solution. Two algorithms are developed to obtain the spatial derivatives determined by a bi-diagonal matrix along a grid line, using fourth order five-point non-centered difference scheme for the wall boundary conditions. Although, both the schemes have the ability to capture dam-break flow with good accuracy, fourth order compact scheme provides better result in the vicinity of shock. The fourth order scheme with low computation and high accuracy provides better result than second order scheme especially in the vicinity of shock. The present model could be a good alternative to the existing explicit MacCormack methods for solving hyperbolic systems, particularly for solving the SWE.

References

[1] I. M. Navon, H.A.Riphagen, An Implicit Compact Fourth-Order Algorithm for Solving the Shallow-Water Equations in Conservation-Law Form. J. Mon. Weather Review, 107 (1979) 1107-1127.

[2] T. Xanthopoulos, C. Koutitas, Numerical simulation of two-dimensional flood wave propagation due to a dam failure. J. Hydraulic Research, 14(4) (1976) 321-331

[3] N. Katopodes, and T. Strelkoff, Computing two-dimensional dam break waves. ASCE J. Hydraulic Division, 104(9) (1978) 1269-1288.

[4] D.L. Fread, J. M. Lewis, FLDWAV, A generalized flood routing model. Proceedings of National Conference on Hydraulic Engineering. Colorado, (1988) 666-673.

[5] V. Bellos, V. Hrissanthou, Numerical simulation of dam-break flood wave. J. European Water, 33 (2011) 45-53.

[6] P.K. Mohapatra, S.M. Bhallamudi, Computation of a dam-break flood wave in channel transitions. Adv. in Water Resources, 19 (3) (1996) 181-187.

[7] M. Rahman, M.H. Chaudhry, Simulation of dam-break flow with grid adaptation. Adv. I n Water Resources, 21 (1998) 1-9.

[8] C. Zoppou, S. Roberts, Numerical solution of the two-dimensional unsteady dam-break Appl. Math. Model, 24 (2000) 457-475.

[9] C. Biscarini, S.D. Francesco, Manciola, P, CFD modeling approach for dam-break studies. J. Hydrol. Earth Syst. Sci., 14 (2010) 705-718.

[10] J. Bagheri, S. K. Das, Modelling of shallow water equations by using higher-order compact scheme with application to dam-break problem. J. Appl. Comp. Math., 2(3) (2013) 1 -9, DOI: 10.4172/2168-9679.1000132

[11] A. Tandel, P.H. Bhathawala, One-dimensional ground water recharge through porous media. Int. J. Adv. Appl. Math. and Mech. 1(1) (2013) 61-67.

[12] A. Kumar, R. Arora, Solutions of the coupled system of Burgers' equations and coupled Klein-Gordon equation by RDT Method. Int. J. Adv. Appl. Math. and Mech. 1(4) (2014) 1-9.

[13] M. Aslefallah, D. Rostamy, A numerical scheme for solving Space-Fractional equation by finite differences theta-method. Int. J. Adv. Appl. Math. and Mech. 1(4) (2014) 1-9.

[14] A. Shah, Li.Yuan, ,A. Khan, Upwind compact finite difference scheme for time-accurate solution of the incompressible Navier-Stokes equations. J. Appl. Math. Comp., 215 (2010) 3201-3213.

[15] S. Abarbanel, A. Kumar, Compact high-order schemes for the Euler equations. J. Scientific Computing, 3 (1988) 275-288.

[16] M.M. Gupta, High accuracy solutions of incompressible Navier-Stokes equations. J. Comp. Phys, 93 (1991) 343-357.

[17] S. K. Lele, Compact finite difference schemes with spectral-like resolution. J. Comp. Phys, 103 (1992) 16-42.

[18] M. Li, T. Tang, Fornberg, B., A compact fourth-order finite difference scheme for the steady incompressible Navier-Stokes equations. Int. J. Numerical Method in Fluids, 20 (1995) 1137-1151.

[19] M. Li, T. Tang, A Compact Fourth-Order Finite Difference Scheme for Unsteady Viscous Incompressible Flows. J. Scientific Computing, 16 (2001) 29-45.

[20] S. K. Pandit, J.C. Kalita, D.C. Dalal, A transient higher order compact schemes for incompressible viscous flows on geometries beyond rectangular. J. Comp. Phys, 225 (2007) 1100-1124.

[21] R.W. Maccormack, The effect of hepervelocity impact cratering. AIAA, (1969) 69- 354.

[22] P.D. Lax,B. Wendroff, Systems of conservation laws. J. Commun. Pure. Appl. Math, 13 (1960) 217-237.

[23] R. Hixon, E. Turkel, Compact implicit MacCormack type schemes with high accuracy. J. Comp. Phys., 158 (2000) 51-70.

[24] J. J. Stoker, Water Waves. New York, Wiley Interscience. (1957).

[25] J. M. Townson, A. H. Al-Salihi, Models of dam-break flow in R-T space. ASCE J. Hydraulic Engineering, 115(5) (1989) 561-575.

[26] R. Garcia, R.A. Kahawaita, Numerical solution of the St.Venant equations with Mack Cormack finite-difference scheme. J. Numerical Method in Fluids, 6 (5) (1986) 259-274.

[27] K.R., Helfrich, C.K. Allen, and L. J. Pratt, Nonlinear Rossby adjustment in a channel. J. Fluid Mech., 390 (1999) 187-222.

[28] C.V. Bellos, J. V. Soulis, J.G. Sakkas, Computation of two-dimensional dam-break induced flows. Adv. in Water Resources, 14 (1) (1991) 31-41.